Biosensors and Bioelectronics 132 (2019) 76–83

Contents lists available at ScienceDirect

Biosensors and Bioelectronics

journal homepage: www.elsevier.com/locate/bios

A shriveled rectangular carbon tube with the concave surface for high-performance enzymatic glucose/O_2 biofuel cells

Zepeng Kang, Yi-Heng P. Job Zhang, Zhiguang Zhu*

Tianjin Institute of Industrial Biotechnology, Chinese Academy of Sciences, 32 West 7th Avenue, Tianjin Airport Economic Area, Tianjin 300308, China

ARTICLE INFO

Keywords:
Rectangular carbon tube
Polypyrrole
Carbonization
Enzymatic biofuel cell
Constant-current discharge

ABSTRACT

In this study, a novel carbon tube was prepared by carbonizing a rectangular polypyrrole (RPPy) tube at a high temperature for the construction of enzymatic biofuel cells with high performance. SEM and TEM images clearly showed that the initial PPy presented a rectangular tube shape, while the carbonized PPy became a shriveled rectangular tube with a concave surface, which might be beneficial for enzyme immobilization and electrochemical applications. The glucose oxidase (GOx)- or laccase (Lac)-modified electrodes based on carbonized RPPy exhibited excellent bioelectrochemical performance. In addition, a biofuel cell (GOx, glucose/O_2, Lac) was assembled, and the open-circuit voltage reached 1.16 V. The maximum power density was measured to 0.350 mW cm^{-2}, which correlated to the gravimetric power density of 0.265 mW mg^{-1} (per mg of GOx) at 0.85 V. The constant-current discharge method was used to further evaluate the continuous discharge capacity. The discharge time reached 49.9 h at a discharge current of 0.2 mA before the voltage was lower than 0.8 V. Furthermore, three of the fabricated biofuel cells in series were able to continually light up a white light-emitting diode (LED) whose turn-on voltage was ca. 2.4 V for more than 48 h. This study suggests that carbonized conducting polymers may become a useful electrode material for the development of enzymatic biofuel cells.

1. Introduction

Enzymatic biofuel cells (EBFCs) consisting of two enzyme-modified electrodes can yield electrical energy from green and renewable fuels (Abdelkader et al., 2011; Abreu et al., 2018; Giroud et al., 2017; Liu et al., 2018; Zhang et al., 2015; Zhu et al., 2014). Numerous studies on this new type of fuel cell have obtained great success (Agnès et al., 2013; Blaik et al., 2016; Bollella et al., 2017; Kang et al., 2017a, 2017b; Lalaoui et al., 2016; Prasad et al., 2014; Qian and Lu, 2014). However, certain aspects of performance (open-circuit voltage, output power density and lifespan) of the current EBFCs could still be improved. These shortcomings can be attributed to the following: i) low enzyme loading on the surface of electrodes, ii) inefficient electron transfer across enzyme-electrode interfaces, iii) inferior stability of enzymatic electrodes (Hui et al., 2017; Zhang et al., 2017). To address these drawbacks, exploring novel electrode materials with excellent physical and chemical properties, especially the highly enzyme-accessible surface area and good electrical conductivity, has been suggested as an effective strategy. In recent years, a plethora of carbon materials, such as carbon nanotube (CNTs) (Eguílaz et al., 2016; Tominaga et al., 2015; Zhang et al., 2017), graphene (Gr) (Guo et al., 2015; Liang et al., 2015; Navaee and Salimi, 2015; Qiu et al., 2017), carbonized polymers (Kang et al., 2017a, 2017c) and three-dimensional (3D) carbon composites (Prasad et al., 2014; Wu et al., 2014; Zhang et al., 2014), have attracted strong interest and been widely applied in the field of EBFCs due to their many advantages, i.e., high specific surface area, excellent electrical conductivity, good biocompatibility and special porous network structures (Kang et al., 2017a; Prasad et al., 2014; Qian and Lu, 2014; Zhang et al., 2017). Conventionally, mingling such kinds of typical carbon nanomaterials, conducting polymers and metal nanomaterials together through chemical bonding or physical absorption has been suggested as an effective method to develop new carbon composites for EBFCs (Fu et al., 2016; Ji et al., 2017; Zhang et al., 2017).

Alternatively, carbonizing the conducting polymers that contain abundant carbon atoms is also effective to explore novel carbon nanomaterials because the morphologies of polymers are diversification and controllability. In the application of storage batteries or supercapacitors, there are abundant reports on carbonized conducting polymers (Zhang et al., 2016; Zhu et al., 2016). Generally, their carbonization temperature was lower than 1000 °C, and the carbonized products were mainly amorphous carbon, which contains many defects, such as a low degree of intralayer binding and high disorder degree. Increasing the carbonization temperature is well known for improving the performance of the products, albeit possibly leading to the collapse

* Corresponding author.
E-mail address: zhu_zg@tib.cas.cn (Z. Zhu).

https://doi.org/10.1016/j.bios.2019.02.044
Received 15 December 2018; Received in revised form 13 February 2019; Accepted 21 February 2019
Available online 23 February 2019
0956-5663/

of the initial morphology. Although such high-temperature carbonized materials own some weakness, they are still promising materials for bioelectrochemical application if their preparation method can be well optimized. For example, Kang et al. first confirmed that the nanofiber-like polyaniline (PANI) would be pyrolyzed to a granular or globular shape when the carbonization temperature was higher than 1000 °C. To maintain its initial morphology, they fabricated a 3D composite of PANI@Gr relying on the strong covalent bonds and carbonized at 1600 °C. As expect, the carbonized PANI still presented the nanofiber-like structure on the surface of Gr. The assembled glucose/O_2 biofuel cell based on $PANI_{1600}$@Gr could output a maximum power density of 0.756 mW cm^{-2} at 0.42 V (Kang et al., 2017c). Later, they prepared a 3D carbon composite of $PANI_{1600}$@CNT for another glucose/O_2 biofuel cell and the maximum power density reached 1.12 mW cm^{-2} at 0.45 V (Kang et al., 2017a). However, there is no study on carbonizing conducting polymer directly without the help of other carbon nanomaterials, nor its use in the EBFCs field.

Beyond the above-mentioned technical problems in exploring novel carbonized conducting polymer-based electrodes, there are still other problems in the study of EBFCs. Generally, the performance of EBFCs is mainly expressed by two characteristics: open-circuit voltage (OCV) and output power density. The output power density is usually measured by linear sweep voltammetry (LSV) (Ji et al., 2017; Xiao et al., 2018; Zhang et al., 2017). Actually, the value obtained from LSV is instantaneous data which varies with the scan rate, so it cannot completely represent the actual performance, such as the continuous discharge capacity. Unfortunately, to our knowledge, there are few reports on the continuous discharge of EBFCs. Furthermore, the unit of power density, mW cm^{-2}, is deficient for meaningful comparison between various reports because the electrode area is usually the geometric area, yet this is not the same as the actual effective surface area or electroactive surface area. Moreover, the actual enzyme loadings applied on the electrodes differ depending on the enzyme immobilization approaches. Therefore, further investigation on continuous discharge capacity and data standardization are desired now.

Herein, a novel shriveled rectangular carbon tube with a concave surface was prepared by carbonizing a rectangular polypyrrole (RPPy) tube at a high temperature under laboratory conditions for the immobilization of GOx and Lac. The direct electron transfer property and direct electro-oxidation of glucose were studied based on the fabricated GOx-modified electrode. In addition, a biofuel cell (GOx, glucose/O_2, Lac) was assembled and the unit of power density mW mg^{-1} (per mg of enzyme) was adopted to characterize its performance. The constant current discharge method was used to further characterize its continuous discharge capacity.

2. Experimental section

2.1. Materials and reagents

GOx (EC 1.1.3.4, from *Aspergillus niger*, ≥ 180 U mg^{-1}), 2,2′-azinobis (3-ethylbenzothiazoline-6-sulfonic acid) diammonium salt (ABTS) and Nafion solution (5 wt%) were purchased from Sigma-Aldrich and used as received. Lac (EC 1.10.3.2, from *Polyporus brumalis* ≥ 30 U mg^{-1}) was a kind gift from Professor Wenxia Jiang's group at Tianjin Institute of Industrial Biotechnology, Chinese Academy of Sciences. Pyrrole (99%), $FeCl_3{\cdot}6H_2O$ (99%), methyl orange (96%), polyvinylpyrrolidone (K29–32, PVP) and β-D-Glucose (99%) were purchased from Aladdin. Conventional reagents were obtained from Sinopharm Chemical Reagent Co., Ltd. All reagents were of analytical grade and used without further purification. Nafion 211 membranes were purchased from DuPont China Holding Co., Ltd. The nickel foam (NiF, 0.5 mm thickness) was purchased from Yiyang Foammetal New Material Co., Ltd. The phosphate buffer solution (PBS, 0.1 M, pH 7.2), Tris-HCl buffer (0.05 M, pH 8.5), Britton-Robison buffer (B-R, 0.1 M, pH 5.0) and sodium acetate buffer (SDA, 0.1 M, pH 5.0, 7.0) were the frequently-used buffers in the experiment. The 0.05 M glucose stock solutions were in PBS and mutarotated at least 24 h before use. All solutions were prepared with the deionized water which was purified with a Millipore-Q purification system (specific resistance > 18.0 MQ cm).

2.2. Instruments

Scanning electron microscopy (SEM) was carried out by using a JSM-6701 field emission SEM instrument (JEOL, Japan) at an accelerating voltage of 10 kV with a Phoenix energy-dispersive X-ray analyzer (NS7, Thermo, USA). Transmission electron microscopy (TEM) images were recorded on a JEOL JEM-2100 microscope, which was operated at an acceleration voltage of 200 kV. The electrochemical performance was measured by an electrochemical workstation CHI 660E (Shanghai Chenhua Instrument Co. Ltd, China). The constant current discharge was conducted by a charge-discharge tester (Wuhan LAND CT2001A Electronics, China).

2.3. Synthesis of rectangular tube PPy and carbonization

The rectangular tube PPy (RPPy) was synthesized by the soft-template method according to a previous report (Kopecká et al., 2014). In brief, 300 mL 40 mM $FeCl{\cdot}6H_2O$ aqueous solution was added slowly into 600 mL 5 mM methyl orange aqueous solution under magnetic stirring and maintained for 10 min. Then, 2.05 mL pyrrole was dropped in the above mixed solution under the magnetic stirring. Lastly, the mixture was placed quietly for 24 h at room temperature. For comparison, a type of circular tube PPy (CPPy) was also synthesized with a different ratio of reagents. Briefly, we only changed the molarity of the methyl orange to 4 mM, and the others remained unchanged.

Carbonization was carried out in a high-temperature tube furnace by gradually heating (at 2 °C min^{-1}) the RPPy and CPPy to each target temperatures of 800, 1000, 1200, 1400, and 1600 °C with the protection of an argon atmosphere. Then, the target temperature was maintained for 3 h. After cooling, the products were abbreviated to $RPPy_x$ and the $CPPy_x$, where x represents the target carbonization temperature. The schematic diagram of the synthetic procedures is shown in Scheme 1.

2.4. Enzyme-modified electrode preparation and electrochemical measurements

A three-electrode system, including a working electrode, an Ag/AgCl reference electrode, and a 1 × 1 cm^2 platinum counter electrode, was used to perform cyclic voltammetry (CV) experiments and enzyme-modified electrode characterization. Beforehand, a glassy carbon electrode (φ 3 mm) was polished according to previous reports (Kang et al., 2017a, 2017c). For the bioanode, first, 6 μL 5 mg mL^{-1} carbonized $RPPy_x$ suspension (prepared by 1 mg mL^{-1} PVP aqueous solution, where the PVP was used as the surfactant) was dropped onto the surface of a cleaned GCE and air-dried. The obtained electrode was designated

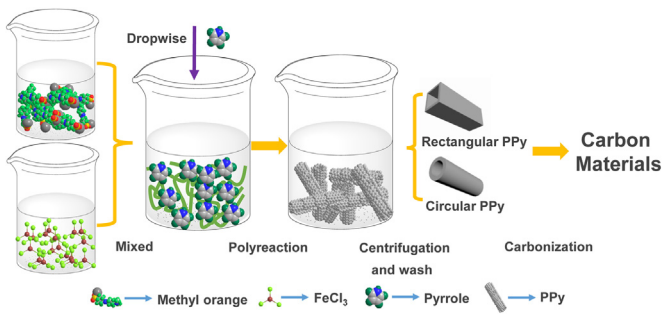

Scheme 1. Schematic diagram of the preparation of carbonized PPy.

as PVP-RPPy$_x$/GCE. Then, 4 μL 20 mg mL^{-1} GOx solution (prepared by the Tris-HCl buffer, pH 8.5) was spread onto the surface of PVP-RPPy$_x$/GCE and placed at 4 °C for 12 h. The obtained electrode was designated as GOx/PVP-RPPy$_x$/GCE. Lastly, 5 μL Nafion solution (1 wt% in 99.99% ethyl alcohol) was spread on the surface of GOx/PVP-RPPy$_x$/GCE and the electrode was placed at 4 °C for 6 h. The final electrode was designated Nafion/GOx/PVP-RPPy$_x$/GCE. The Nafion/GCE, Nafion/GOx/GCE, Nafion/PVP-RPPy$_x$/GCE and Nafion/GOx/PVP-CPPy$_x$/GCE were prepared for control experiments.

A 0.5 × 0.5 cm^2 nickel foam (NiF) was also utilized as the substrate electrode. Before being used, the NiF slices were successively cleaned with the 1 M H_2SO_4 aqueous solution, deionized water, ethyl alcohol and deionized water by the ultrasonic method for 10 min. Then, 50 μL 5 mg mL^{-1} carbonized RPPy$_x$ suspension was dropped on the surface of a cleaned NiF and air-dried. The obtained electrode was designated PVP-RPPy$_x$/NiF. Then, 10 μL 20 mg mL^{-1} Lac solution (prepared by the SDA buffer, pH 5.0) was spread on the surface of PVP-RPPy$_x$/NiF, and the electrode was placed at 4 °C for 12 h. The obtained electrode was designated Lac/PVP-RPPy$_x$/NiF. A bioanode of GOx/PVP-RPPy$_x$/NiF was also fabricated through the same processes. All the prepared enzyme modified electrodes were stored at 4 °C when not in use.

The Nyquist plot was obtained by performing electrochemical impedance spectroscopy at open circuit potential over an AC frequency range of 100 kHz to 100 mHz, with a sinusoidal perturbation of 5 mV. The equivalent circuit consisted of a parallel resistor–capacitor element with a Warburg element. ZView (version 3.1c, Scribner Associates, Inc. USA) was employed for equivalent circuit model fittings.

2.5. EBFCs assembled and performance measurements

An EBFC (GOx, glucose/O_2, Lac) was constructed with two compartments by using the acrylic glass and separated by the Nafion 211 membrane. For the bioanode, a piece of 2 × 2 cm^2 NiF was as the substrate electrode, and 500 μL 5 mg mL^{-1} carbonized RPPy$_x$ suspension was dropped onto the surface of the NiF electrode and air-dried. Then, 150 μL 20 mg mL^{-1} GOx solution was spread on the surface of the electrode and placed at 4 °C for 24 h. The biocathode was made in a similar way, but using Lac instead. The electrolyte of the anodic compartment was 50 mL Ar-saturated 0.1 M SDA (pH 5.0) with 0.05 M glucose. The cathodic compartment was filled with 50 mL 0.1 M B-R buffer (pH 5.0) with 0.5 mM ABTS and continuously bubbled with oxygen. The performance of the glucose EBFC was measured through the manual variation of circuit resistance while measuring output voltage (Scheme S1) and a charge-discharge tester.

3. Results and discussion

3.1. Microscopic and spectroscopic characterization

Fig. 1 shows the SEM and TEM images of the PPy before and after carbonization. As seen in Fig. 1A and A$_1$, the RPPy presented a distinct rectangular tube with four planar surfaces, while the CPPy was a typical

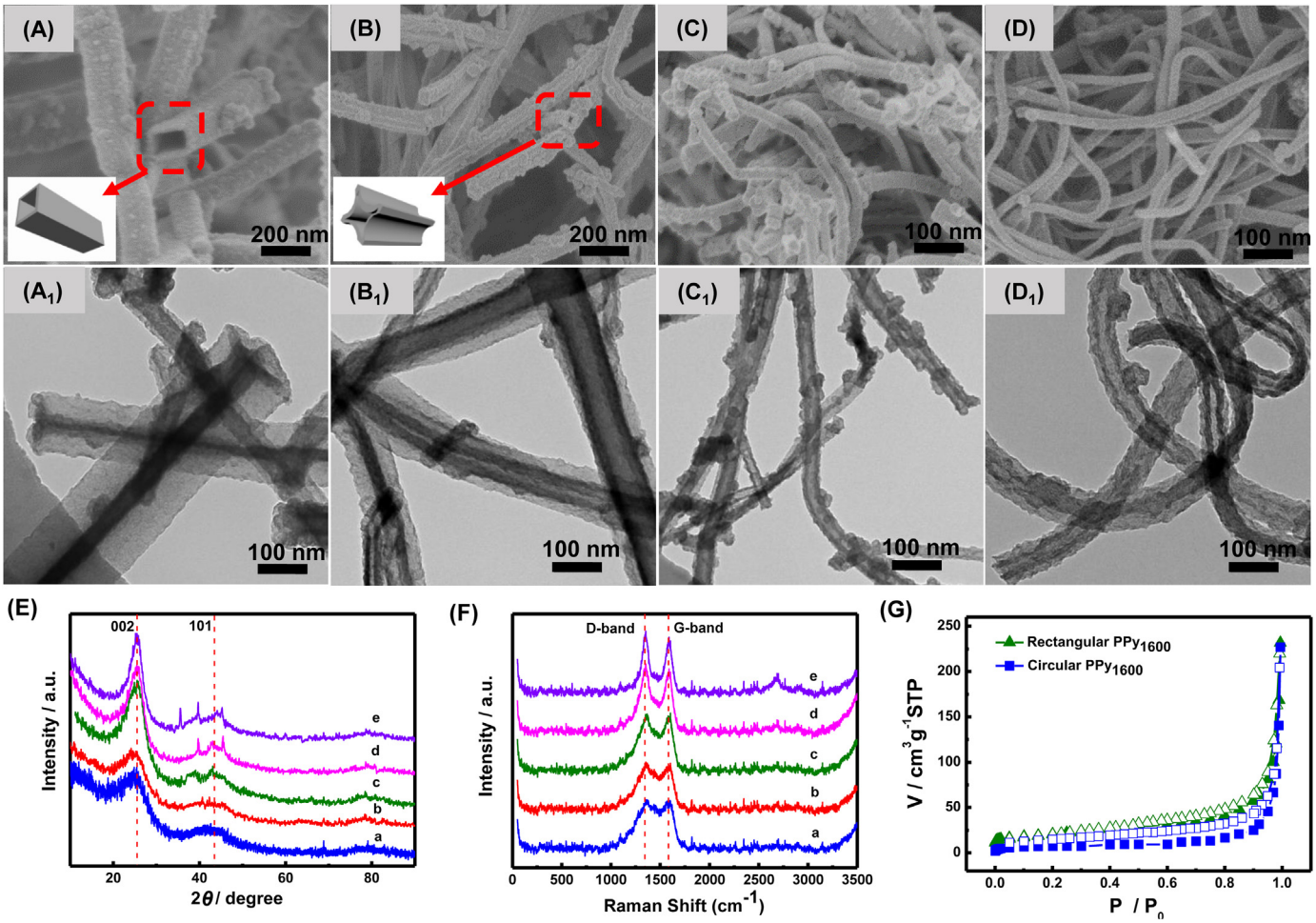

Fig. 1. Characterization of the RPPy and CPPy before and after carbonized at 1600 °C. SEM images of (A) RPPy, (B) RPPy$_{1600}$, (C) CPPy and (D) CPPy$_{1600}$; TEM images of (A$_1$) RPPy, (B$_1$) RPPy$_{1600}$, (C$_1$) CPPy and (D$_1$) CPPy$_{1600}$. (E) XRD pattern and (F) Raman spectra of (a) RPPy$_{800}$, (b) RPPy$_{1000}$, (c) RPPy$_{1200}$, (d) RPPy$_{1400}$ and (e) RPPy$_{1600}$. (G) N_2 adsorption–desorption isotherms for the obtained samples of RPPy$_{1600}$ and CPPy$_{1600}$.

circular tube with an arched surface (Fig. 1C and C_1). The RPPy had a rectangular cavity and was very similar to the schematic diagram, which corresponded to a previous report (Kopecká et al., 2014). Interestingly, the RPPy in Fig. 1B shows a shriveled rectangular tube structure with a concave surface after carbonization at 1600 °C, which might be caused by gas emission, such as CO, CH_4, etc., during the calcination process (Kang et al., 2017c; Zhu et al., 2016). The schematic diagram in Fig. 1B can exhibit a visual reified morphology for understanding. The SEM images of other products, $RPPy_{800}$, $RPPy_{1000}$, $RPPy_{1200}$, and $RPPy_{1400}$, are shown in Fig. S1, and all of them presented the same morphologies. These results demonstrated that the RPPy had the inferior thermostability at the high temperature. In Fig. $1B_1$, the corner angles and the concave surfaces can be clearly seen, which might benefit the immobilization of enzyme. In the control experiment, the $CPPy_{1600}$ in Fig. 1D and D_1 still presented the typical circular tube, which was attributed to the more stable structure of arched surface.

Fig. 1E shows the XRD results of the chemical structure and composition of the $RPPy_x$. Two broad peaks were observed at 26.0° and 43.0° in each curve, which can be attributed to the (002) and (101) planes of the hexagonal graphite structure, respectively (Kang et al., 2017c; Zhu et al., 2016). The peaks presented broad features, indicating that the $RPPy_x$ had the amorphous carbon feature with a low degree of graphitization crystallinity. The peak at approximately 26.0° became more incisive and narrow with the increasing carbonization temperature, suggesting that the degree of graphitization crystallinity became better. The peaks at approximately 43.0° also became more distinct with increasing carbonization temperature, indicating a higher degree of intralayer binding at the high temperatures, which can improve the electronic conductivity of carbide materials (Zhu et al., 2016). The improvement of graphitization was further demonstrated by Raman spectra (Fig. 1F). Two obvious peaks were observed at each curve $a \sim e$ and their full width at half maximum decreased with increasing carbonization temperature. The peak at 1350 cm^{-1} (D-band) was attributed to the vibration of sp^2-hybridized carbon atoms, and the peak at 1580 cm^{-1} (G-band) was attributed to the vibration of sp^3-hybridized carbon atoms (Kang et al., 2017b; Zhang et al., 2014). Usually, the D-band characterizes the disorder degree and the integral area ratio of D-band and G-band (I_D/I_G) can be used to evaluate the defect degree (Zhu et al., 2016). The full width at half maximum of the D-band decreased more obvious than the G-band, and the integral area ratio of I_D/I_G decreased from 2.32 to 1.06 as the carbonization temperature increased from 800 °C to 1600 °C, demonstrating that the degree of graphitization crystallinity increased and there was less disorder in the products carbonized at the higher temperature. In addition, the specific surface areas of the $RPPy_{1600}$ and $CPPy_{1600}$ were characterized by using N_2 adsorption-desorption isotherms and shown in Fig. 1G. The specific surface areas of $RPPy_{1600}$ and $CPPy_{1600}$ were 88.315 $m^2\ g^{-1}$ and 64.767 $m^2\ g^{-1}$, respectively, which were very close to the CNTs (Peigney et al., 2001), indicating that the $RPPy_{1600}$ had similar properties to CNTs. The specific surface area of $RPPy_{1600}$ was larger than $CPPy_{1600}$, possibly because of the special concave surface. The average pore diameter of RPPy and CPPy were 5.187 nm and 1.356 nm, respectively. The cumulative pore volume of RPPy and CPPy were 1.615 and 1.2 $cm^3\ g^{-1}$ (Fig. S2). All these results demonstrate that the $RPPy_{1600}$ and $CPPy_{1600}$ might be promising supporting materials for fabricating enzymatic electrodes.

3.2. The electrochemical properties of GOx base on $RPPy_x$

Next, the cyclic voltammograms (CVs) of Nafion/GOx/PVP-$RPPy_x$/GCE electrodes, where x represents the carbonization temperature (°C), which were (curve a) $x = 800$, (curve b) $x = 1000$, (curve c) $x = 1200$, (curve d) $x = 1400$, (curve e) $x = 1600$, in 0.1 M N_2-saturated PBS (pH 7.2) at a scan rate of 50 mV s^{-1} were conducted (Fig. 2A). Obviously, a pair of well-defined redox peaks was displayed in each curve, suggesting that all the GOx-modified electrode had an electroactive substance. A larger leveled current separation of the CV of Nafion/GOx/PVP-$RPPy_{800}$/GCE was observed and it should be ascribed to the pseudocapacitive current because of the impurities, such as N atom, contained in the $RPPy_{800}$. The capacitance current decreased first and then became barely unchanged with increasing carbonization temperature, indicating that the conductivity of $RPPy_x$ was improved, especially at the higher carbonization temperature. The redox peak separation ($\triangle E_P$) of the curve e was the minimum value of ca. 53 mV, indicating a highly-efficient electron transfer rate.(Zhao et al., 2015) Fig. 2B shows the Nyquist plot of Nafion/GOx/PVP-$RPPy_x$/GCE electrodes in 0.1 M N_2 saturated PBS (pH 7.2). Distinctly, a semicircle in the high-frequency region and a straight line in the low-frequency region were observed in each electrochemical impedance spectroscopy curve. Generally, the semicircle diameter is used to estimate the interfacial electron transfer resistance (R_{ct}) between the GOx and the electrode (Kang et al., 2009). As shown in Fig. 2B, with increasing carbonization temperature, R_{ct} tended to get smaller, indicating the conductivity of $RPPy_x$ became better, which was in accordance with the results of Fig. 2A. Hence, the Nafion/GOx/PVP-$RPPy_{1600}$/GCE electrode was used as the model electrode in the subsequent experiments. Fig. 2C shows the CVs of (curve a) Nafion/GCE, (curve b) Nafion/GOx/GCE, (curve c) Nafion/PVP-$RPPy_{1600}$/GCE, (curve d) Nafion/GOx/PVP-$CPPy_{1600}$/GCE and (curve e) Nafion/GOx/PVP-$RPPy_{1600}$/GCE electrodes in 0.1 M N_2 saturated PBS (pH 7.2) at a scan rate of 50 mV s^{-1}. Obviously, no redox peaks were observed in curve a, b or c, while there was a pair of clear redox peaks in both curves d and e, indicating that the redox peaks were attributed to the GOx(FAD/$FADH_2$) (Liu et al., 2007). The reaction mechanism of GOx without the interference of O_2 was reported previously and is shown below (Kang et al., 2017b; Tasviri et al., 2011):

$$GOx(FAD) + 2H^+ + 2e \leftrightarrow GOx(FADH_2) \quad (1)$$

In addition, the peak current of curve d was slightly larger than curve e, indicating there was slightly more active GOx on the surface of Nafion/GOx/PVP-$RPPy_{1600}$/GCE, which was ascribed to the concave surface of $RPPy_{1600}$. This result further suggested that $RPPy_{1600}$ could be a better electrode material for the immobilization of electroactive GOx than $CPPy_{1600}$. Based on this result, we speculated that the direct electron transfer (DET) between the GOx and the electrode may possibly occur. However, several reports put forth opposite views (Philip and Bartletta, 2018; Wooten et al., 2014). They considered that the observed redox peaks of CV resulted from the free FAD that usually exists in the majority of commercial GOx. Supporting evidence was that their GOx-modified electrode did not respond to the glucose in the O_2-free electrolyte.

To gain better evidence that the immobilized GOx based on $RPPy_{1600}$ can undergo DET, we conducted an experiment for the direct electrocatalytic oxidation of glucose in O_2-free electrolyte based on a new GOx-modified electrode. Here, the GOx-modified electrode was changed by the GOx/PVP-$RPPy_{1600}$/NiF to exclude the influence of the Nafion membrane on the mass transfer between the bioanode and the electrolyte because the Nafion membrane only permits the H^+ to cross itself. The incubation pH of GOx was also different from that in (Wooten et al., 2014). As shown in Fig. 2D, the oxidation current of curve a increased obviously compared with curve b, while no current changes were observed in curves a or b in Fig. 2E, suggesting that the GOx/PVP-$RPPy_{1600}$/NiF might directly respond to the glucose. The electrochemical reaction mechanism is as follows (Prasad et al., 2014):

$$GOx(FAD) + glucose \rightarrow GOx(FADH_2) + gluconolactone \quad (2)$$

$$GOx(FADH_2) \rightarrow GOx(FAD) + 2H^+ + 2e \quad (3)$$

The increase of oxidation current of curve a in Fig. 2D was attributed to reaction 2, which produced more GOx($FADH_2$) and resulted in reaction 3. In addition, the more positive the potential the more obvious the oxidation current (Fig. 2F). This result demonstrate that immobilized GOx can undergo DET because the free FAD can not oxidize

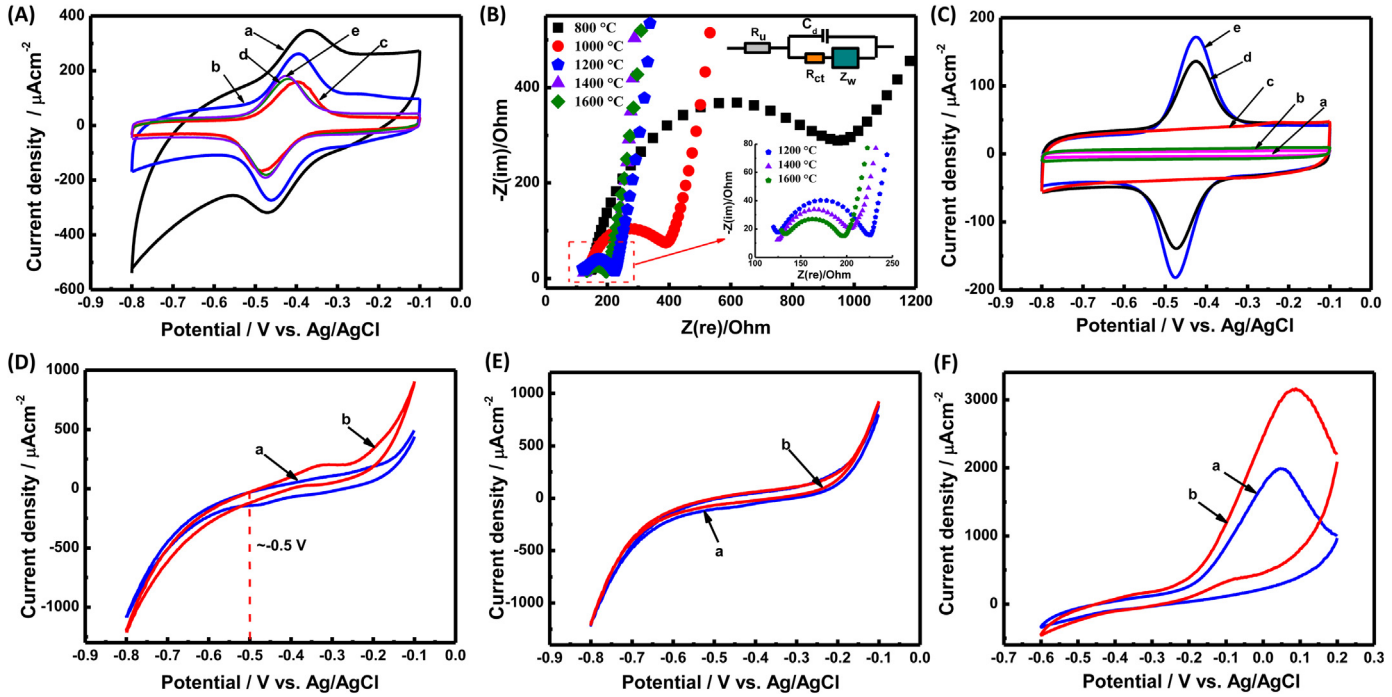

Fig. 2. (A) CVs and (B) Nyquist plot of Nafion/GOx/PVP-RPPy$_x$/GCE, (a) x = 800, (b) x = 1000, (b) x = 1200, (d) x = 1400, (e) x = 1600 °C; (C) CVs of (a) Nafion/GCE, (b) Nafion/GOx/GCE, (c) Nafion/PVP-RPPy$_{1600}$/GCE, (d) Nafion/GOx/PVP-CPPy$_{1600}$/GCE and (e) Nafion/GOx/PVP-RPPy$_{1600}$/GCE electrodes; All experiments were conducted in 0.1 M N_2-saturated PBS (pH 7.2); scan rate: 50 mVs^{-1}. CVs of (D and F) GOx/PVP-RPPy$_{1600}$/NiF and (E) PVP-RPPy$_{1600}$/NiF in 0.1 M N_2-saturated acetate buffer (pH 5.0) (a) without or (b) with 0.05 M glucose; scan rate: 10 mV s^{-1}.

the glucose. It is well known that the testing conditions, such as the incubation pH of GOx, the immobilization methods, the property of the carrier materials and the electrolyte pH, can influence the electrochemical performance of the final GOx-modified electrode. At present, what factor plays the decisive role is not clear and should be further synthetically studied. Based on the DET theory, the onset oxidation potential of glucose was ca. −0.5 V which was very near the redox-active potential of GOx (Prasad et al., 2014). This result is desired for increasing the open circuit voltage of a whole glucose/O_2 biofuel cell consisting of a bioanode and a biocathode.

3.3. The electrochemical properties of Lac based on RPPy$_{1600}$

As for the biocathode, Lac was selected because it is a typical enzyme for oxygen reduction and the catalytic mechanism is well known (Kang et al., 2017a; Prasad et al., 2014). In our system, ABTS was introduced to promote the electron transfer between the Lac and the electrode to exclude the influence of the biocathode on the performance of the whole glucose/O_2 biofuel cell later. Fig. 3 shows the CVs of Lac/PVP-RPPy$_{1600}$/NiF in (curve *a*) 0.1 M N_2-saturated B-R buffer (pH 5.0), (curve *b*) 0.1 M O_2-saturated B-R buffer (pH 5.0), (curve *c*) 0.1 M N_2-saturated B-R buffer containing 0.5 mM ABTS (pH 5.0) and (curve *d*) 0.1 M O_2-saturated B-R buffer containing 0.5 mM ABTS (pH 5.0) at a scan rate of 10 mV s^{-1}. Few variations were observed in curves *a* and *b*, indicating that this Lac modified electrode had no electrocatalytic reduction ability of oxygen. However, the reduction current of curve *d* sharply increased compared with curve *c* and the electrocatalytic reduction potential of oxygen started from ca. 0.65 V which was very close to the theoretical value (Prasad et al., 2014). These results indicate that the Lac modified electrode based on RPPy$_{1600}$ had excellent bioelectrocatalytic activity for oxygen reduction with the help of ABTS.

3.4. The performance of the assembled EBFCs

A glucose/O_2 biofuel cell consisting of the GOx/PVP-RPPy$_{1600}$/NiF as the bioanode and the Lac/PVP-RPPy$_{1600}$/NiF as the biocathode was assembled and its performance was evaluated through the manual variation of the circuit resistance while measuring output voltage for power density and a charge-discharge tester for continuous discharge capacity. As shown in Fig. 4A, the open-circuit voltage (U_{OCV}) reached ~1.16 V, corresponding to the sum of open-circuit potentials of the bioanode and the biocathode (Fig. S3). This value was very close to the theoretical potential difference between the O_2/H_2O couple and the gluconolactone/glucose couple at thermodynamic equilibrium, suggesting the efficient electrocatalytic activity of GOx and Lac based on RPPy$_{1600}$ (Prasad et al., 2014). The conventional maximum power density was calculated to be 0.350 mW cm^{-2} (per geometric area of bioanode), which correlated to the gravimetric power density of 0.265 mW mg^{-1} (per mg of GOx) at 0.85 V. Here, the weight of GOx was the apparent mass, i.e., the actual usage amount in the preparation

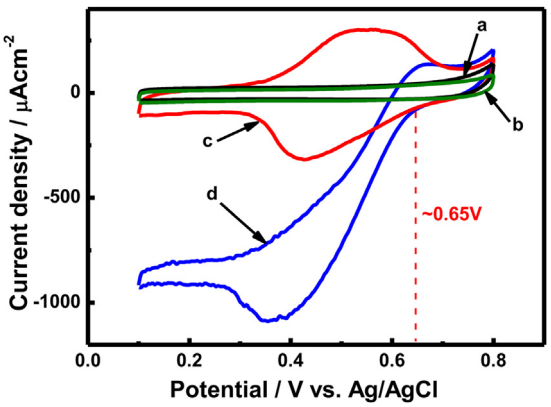

Fig. 3. CVs of Lac/PVP-RPPy$_{1600}$/NiF in (a) 0.1 M N_2-saturated B-R buffer (pH 5.0), (b) 0.1 M O_2-saturated B-R buffer (pH 5.0), (c) 0.1 M N_2-saturated B-R buffer containing 0.5 mM ABTS (pH 5.0), (d) 0.1 M O_2-saturated B-R buffer containing 0.5 mM ABTS (pH 5.0). Scan rate: 10 mV s^{-1}.

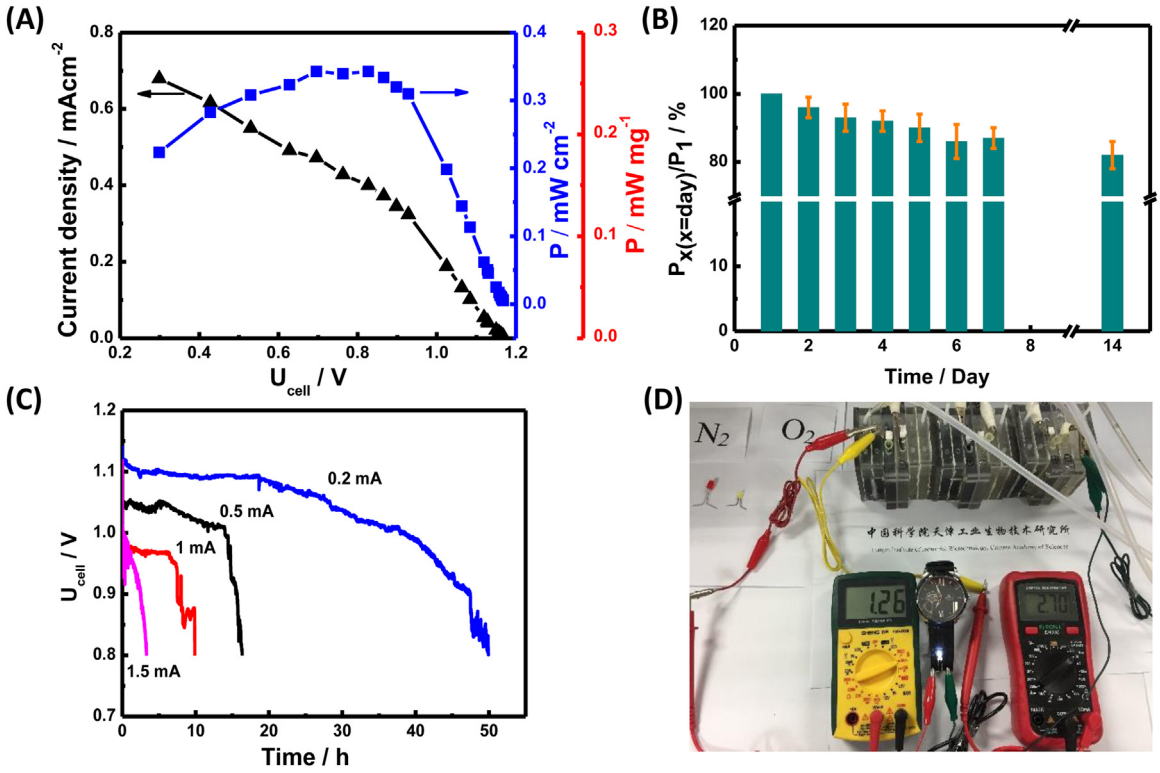

Fig. 4. (A) The power output characteristics of EBFCs (GOx, glucose/O_2, Lac) obtained by the external resistance method. (B) Stability test of the biofuel cell. The value of power density control (100%) corresponds to initial value. (C) Discharge curves of EBFCs (GOx, glucose/O_2, Lac) at a constant current of 0.2 mA, 0.5 mA, 1 mA and 1.5 mA in a voltage range of 1.2–0.8 V. (D) A white light emitting diode (LED) powered by three EBFCs in series.

process of GOx/PVP-RPPy$_{1600}$/NiF. To highlight the high performance of this biofuel cell, a comparison of several relevant studies on glucose/O_2 biofuel cell is listed in Table 1. The OCV was much larger than the others and the reasons are provided in the Section 3.2. For the comparison of the maximum power density, however, there was no uniform evaluation criterion for meaningful comparison of these reports because the actual effective areas of the various electrodes were different, while the power density was usually obtained by using the geometric area. As early as 2015, Campbell et al. reported a unit of power density, mW mg^{-1}, to characterize their EBFCs in terms of gravimetric power density by per mass of catalyst and they considered that this was important for meaningful comparison between studies (Campbell et al., 2015). In addition, the testing method also played a critical role in the measurement of power density, especially for that using the LSV method, which obtained data that varied with the scan rate. Therefore, it is necessary to normalize the evaluation system of EBFCs not only in evaluation criteria but also in the testing method.

The storage stability was evaluated by recording the power density once a day and the glucose/O_2 biofuel cell was placed at 4 °C when not in use (Fig. 4B). After 14 days, the power density was still 82.02%, corresponding to the initial values, indicating the high stability of this glucose/O_2 biofuel cell. However, this result does not truly reflects its continuous discharge capacity. Very recently, Abreu et al. used an external resistor to test the continuous discharge capacity of their EBFCs and the EBFCs could discharge 90 min at a resistance of 3 kΩ (Abreu et al., 2018). On the basis of that study, the constant-current discharge method was used to further evaluate the continuous discharge capacity in this work. As shown in Fig. 4C, the continuous discharge time was nearly 49.9 h at a discharge current of 0.2 mA (0.1 mA mg^{-1}, per mg of GOx) in a voltage range of 1.2–0.8 V. The fluctuation of U_{cell} was likely to be the rolling mass transfer caused by bubbling the N_2 or O_2 and the smooth drop might be ascribed to the decrease in glucose concentration. After that, the EBFC was refueled three times and discharged at three currents of 0.5 mA, 1.0 mA and 1.5 mA, respectively. Obviously, the discharge time decreased gradually with increasing discharge current and all the curves presented a dramatic drop after a period of time, which might be because the inherent catalytic efficiency could not satisfy the power output at a larger discharge current. These results indicate that this glucose/O_2 biofuel cell would revive when glucose was refueled.

The real power capacity of the glucose/O_2 biofuel cell was also demonstrated by powering a light-emitting diode (LED) and the practical application was recorded. Fig. 4D shows that three glucose/O_2 biofuel cells in series were able to light up a white LED whose turn-on voltage was ca. 2.4 V for more than 48 h and the momentary pictures are shown in Fig. S4. The initial open-circuit voltage was high to 3.56 V and the starting output power was 3.4 mW. Subsequently, the working voltage was maintained at ~2.66 V and the discharge current decreased gradually with time. The raised discharge current at 12 h was due to refilling glucose solution and the open-circuit voltage still reached 3.29 V after 48 h, suggesting that this glucose/O_2 biofuel cell had excellent long power supply ability and repeatability.

4. Conclusion

The present study developed a shriveled rectangular carbon tube with the concave surface by carbonizing a rectangular tube polypyrrole (RPPy) at a high temperature. GOx- and Lac-modified electrodes were fabricated based on RPPy$_{1600}$ and their electrochemical properties were studied. Both the GOx- and the Lac-modified electrode exhibited the excellent electrocatalytic properties for glucose oxidation and oxygen reduction, respectively, which may be ascribed to the unique morphological and physical features of RPPy$_{1600}$. A biofuel cell (GOx, glucose/O_2, Lac) was assembled and the open-circuit voltage reached 1.16 V. Consequently, the maximum power density was measured to 0.350 mW cm^{-2}, which correlated with the gravimetric power density of 0.265 mW mg^{-1} (per mg of GOx) at 0.85 V. The gravimetric power density by per mass of catalyst will be important for meaningful

Table 1
Performance comparison between different glucose/O_2 biofuel cells reported previously.

Anode	Cathode	Electron transfer	OCV (V)	P_{max} (mW cm^{-2})	P_{max} (mW mg^{-1})	Testing method	Ref
GOx/PVP-RPPy$_{1600}$/NiF	Lac/PVP-RPPy$_{1600}$/NiF + ABTS	Anode: DET Cathode: MET	1.16	0.350	0.265	External resistance	This work
GOx/Gr/MWCNTs cogel	BOD/Gr/MWCNTs cogel	Anode: DET Cathode: DET	0.61	0.190	0.140	External resistance	(Campbell et al., 2015)
Nafion/GOx/Fc/3D-GN/GCE	Nafion/Lac/3D-GNs-PTCA-DA/GCE	Anode: MET Cathode: MET	0.40	0.112	–	External resistance	(Zhang et al., 2014)
GOx/PPy/Fc	Pt/C	Anode: MET Cathode: DET	0.416	0.13	–	LSV Scan rate: 1 mV s^{-1}	(Crepaldi et al., 2014)
CNTs-Fc/SF-GOx/GCE	Pt/C	Anode: MET Cathode: DET	0.48	0.051	–	LSV Scan rate: 1 mV s^{-1}	(Liu et al., 2012)
GOx/Fe_3O_4/CNF	BOD/Fe_3O_4/CNF	Anode: DET Cathode: DET	0.68	0.126	–	LSV Scan rate: 1 mV s^{-1}	(Ji et al., 2017)
GOx/Gr/AuNPs/NiF + FcCA	Lac/Gr/AuNPs/NiF	Anode: MET Cathode: DET	0.64	2.84	–	LSV Scan rate: 10 mV s^{-1}	(Hui et al., 2017)
Nafion/GOx/PANI$_{1600}$@CNTs/GCE	Nafion/Lac/PANI$_{1600}$@CNTs/GCE + ABTS	Anode: DET Cathode: DET	0.78	1.12	–	LSV Scan rate: 20 mV s^{-1}	(Kang et al., 2017a)

DET: direct electron transfer; MET: mediated electron transfer; MWCNTs: multiwalled carbon nanotube; Fc: ferrocene; GN: graphene network; PTCA: perylene tetracarboxylic acid; DA: dopamine; SF: silk film; CNF: carbon nanofiber; AuNPs: gold nanoparticle.

comparison between studies. In addition, the constant-current discharge method was used to further evaluate the continuous discharge capacity, and the discharge time reached up to 49.9 h at a discharge current of 0.2 mA before the voltage dropped to 0.8 V. Three of the fabricated biofuel cells in series were able to continually light up a white light-emitting diode (LED) whose turn on voltage was ca. 2.4 V for more than 48 h. This study demonstrated the potential of carbonized conducting polymers without the aid of other carbon nanomaterials to immobilize electroactive enzymes and discussed some problems existing in the evaluation system of EBFCs. Future work should be focused on the standardization of the evaluation system and the practical application of high-performance EBFCs.

CRediT authorship contribution statement

Zepeng Kang: Methodology, Investigation, Formal analysis, Writing - original draft, Writing - review & editing. **Yi-Heng P. Job Zhang:** Conceptualization. **Zhiguang Zhu:** Conceptualization, Methodology, Supervision, Writing - original draft, Writing - review & editing, Funding acquisition.

Acknowledgments

This work was supported by the Tianjin Institute of Industrial Biotechnology, Chinese Academy of Sciences (ZDRW-ZS-2016-3S), the National Natural Science Foundation of China (21706273, 21878324) and the CAS Pioneer Hundred Talent Program (Type C, reference # 2016-081). We also thank Professor Wenxia Jiang in our institute for the kindly gift of their Laccase.

Notes

The authors declare no competing financial interest.

Declaration of interests

None.

Appendix A. Supporting information

Supplementary data associated with this article can be found in the online version at doi:10.1016/j.bios.2019.02.044.

References

Abdelkader, Z., Chantal, G., Le, G.A., Michael, H., Philippe, C., Serge, C., 2011. Nat. Commun. 2 (2), 370.
Abreu, C., Nedellec, Y., Ondel, O., Buret, F., Cosnier, S., Goff, A.L., Holzinger, M., 2018. J. Power Sources 392, 176–180.
Agnès, C., Reuillard, B., Le Goff, A., Holzinger, M., Cosnier, S., 2013. Electrochem. Commun. 34, 105–108.
Blaik, R.A., Lan, E., Huang, Y., Dunn, B., 2016. ACS Nano 10 (1), 324–332.
Bollella, P., Ludwig, R., Gorton, L., 2017. Appl. Mater. Today 9, 319–332.
Campbell, A.S., Jeong, Y.J., Geier, S.M., Koepsel, R.R., Russell, A.J., Islam, M.F., 2015. ACS Appl. Mater. Interfaces 7 (7), 4056–4065.
Crepaldi, L.B., Neto, S.A., Cardoso, F.P., Ciancaglini, P., De Andrade, A.R., 2014. Electrochim. Acta 136, 52–58.
Eguílaz, M., Gutiérrez, A., Rivas, G., 2016. Sens. Actuators B 225, 74–80.
Fu, Y.B., Liu, Z.H., Su, G., Zai, X.R., Ying, M., Yu, J., 2016. Fuel Cells 16 (3), 377–383.
Giroud, F., Sawada, K., Taya, M., Cosnier, S., 2017. Biosens. Bioelectron. 87, 957–963.
Guo, J., Zhang, T., Hu, C., Fu, L., 2015. Nanoscale 7 (4), 1290–1295.
Hui, Y., Ma, X., Qu, F., Chen, F., Chen, Y., 2017. J. Electrochem. Soc. 164 (13), G112–G120.
Ji, Y., Gai, P., Feng, J., Wang, L., Zhang, J.R., Zhu, J.J., 2017. J. Mat. Chem. A 5, 22.
Kang, X., Wang, J., Wu, H., Aksay, I.A., Liu, J., Lin, Y., 2009. Biosens. Bioelectron. 25 (4), 901–905.
Kang, Z., Jiao, K., Cheng, J., Peng, R., Jiao, S., Hu, Z., 2017a. Biosens. Bioelectron. 101, 60–65.
Kang, Z., Jiao, K., Peng, R., Hu, Z., Jiao, S., 2017b. RSC Adv. 7 (20), 11872–11879.
Kang, Z., Jiao, K., Xu, X., Peng, R., Jiao, S., Hu, Z., 2017c. Biosens. Bioelectron. 96, 367.
Kopecká, J., Kopecký, D., Vrňata, M., Fitl, P., Stejskal, J., Trchová, M., Bober, P., Morávková, Z., Prokeš, J., Sapurina, I., 2014. RSC Adv. 4 (4), 1551–1558.

Lalaoui, N., David, R., Jamet, H., Holzinger, M., Le Goff, A., Cosnier, S., 2016. ACS Catal. 6 (7), 4259–4264.
Liang, B., Guo, X., Fang, L., Hu, Y., Yang, G., Zhu, Q., Wei, J., Ye, X., 2015. Electrochem. Commun. 50, 1–5.
Liu, B., Yan, C., Si, W., Sun, X., Lu, X., Ansorge-Schumacher, M., Schmidt, O.G., 2018. Small 14 (13), 1870058.
Liu, J., Zhang, X., Pang, H., Liu, B., Zou, Q., Chen, J., 2012. Biosens. Bioelectron. 31 (1), 170–175.
Liu, Q., Lu, X., Li, J., Yao, X., Li, J., 2007. Biosens. Bioelectron. 22 (12), 3203–3209.
Navaee, A., Salimi, A., 2015. J. Mat. Chem. A 3 (14), 7623–7630.
Peigney, A., Laurent, C., Flahaut, E., Bacsa, R.R., Rousset, A., 2001. Carbon 39 (4), 507–514.
Philip, N., Bartletta, F.A.A.-L., 2018. J. Electroanal. Chem. 819, 26–37.
Prasad, K.P., Chen, Y., Chen, P., 2014. ACS Appl. Mater. Interfaces 6 (5), 3387–3393.
Qian, L., Lu, L., 2014. RSC Adv. 4 (72), 38273.
Qiu, H.J., Guan, Y., Luo, P., Wang, Y., 2017. Biosens. Bioelectron. 89 (Pt 1), 85–95.
Tasviri, M., Rafiee-Pour, H.-A., Ghourchian, H., Gholami, M.R., 2011. J. Mol. Catal. B: Enzym. 68 (2), 206–210.
Tominaga, M., Sasaki, A., Togami, M., 2015. Anal. Chem. 87 (10), 5417–5421.
Wooten, M., Karra, S., Zhang, M., Gorski, W., 2014. Anal. Chem. 86 (1), 752–757.
Wu, Y., Guo, C., Li, N., Ji, L., Li, Y., Tu, Y., Yang, X., 2014. Electrochim. Acta 146, 386–394.
Xiao, X., Siepenkoetter, T., Conghaile, P.Ó., Leech, D., Magner, E., 2018. ACS Appl. Mater. Interfaces 10 (8), 7107–7116.
Zhang, F.-F., Wang, C.-L., Huang, G., Yin, D.-M., Wang, L.-M., 2016. RSC Adv. 6 (31), 26264–26270.
Zhang, H., Zhang, L., Han, Y., Yu, Y., Xu, M., Zhang, X., Huang, L., Dong, S., 2017. Biosens. Bioelectron. 97, 34–40.
Zhang, L., Bai, L., Xu, M., Han, L., Dong, S., 2015. Nano Energy 11 (12), 48–55.
Zhang, Y., Chu, M., Yang, L., Tan, Y., Deng, W., Ma, M., Su, X., Xie, Q., 2014. ACS Appl. Mater. Interfaces 6 (15), 12808–12814.
Zhao, R., Liu, X., Zhang, J., Zhu, J., Wong, D.K.Y., 2015. Electrochim. Acta 163, 64–70.
Zhu, J., Xu, Y., Zhang, Y., Feng, T., Wang, J., Mao, S., Xiong, L., 2016. Carbon 107, 638–645.
Zhu, Z., Kin Tam, T., Sun, F., You, C., Percival Zhang, Y.H., 2014. Nat. Commun. 5, 3026.